Analytical approach to dynamics of reverse saturable absorbers

A. Kobyakov, D. J. Hagan, and E. W. Van Stryland

School of Optics, Center for Research and Education in Optics and Lasers, University of Central Florida, 4000 Central Florida Boulevard, Orlando, Florida 32816-2700

Received March 27, 2000; revised manuscript received July 11, 2000

We develop an analytical approach to the dynamics of band populations of reverse saturable absorbers modeled by the three-level approximation of the five-level rate equations. We find high-accuracy approximate solutions to these rate equations, taking into account the temporal shape of the incident laser pulse for different regimes of excitation. The results obtained are confirmed by direct numerical integration of the rate equations and are verified by solution of the full system of the rate and the propagation equations. The validity ranges of the approximations are determined. We also prove that for input pulses that are much longer than the lifetime of the first excited state the ground-state depletion obeys the same functional dependence on the input fluence as in the case of rectangular input pulses. The dynamics of the excited states, however, explicitly depends on the pulse shape. We quantitatively estimate the effect of various parameters on the nonlinear absorption coefficient and discuss implementation of the approach by a beam propagation method to reduce the computational time. © 2000 Optical Society of America [S0740-3224(00)01711-2]

OCIS codes: 190.4180, 140.3360, 190.4710.

1. INTRODUCTION

During several recent years considerable efforts have been put forth to study the mechanisms of optical power limiting, synthesize new materials, and develop devices with advanced properties. Optical limiters are used to protect sensors, including human eyes and other sensitive optical elements, from laser-induced damage. The desired transmittance of such an optical element is inherently nonlinear; i.e., the material should be highly transparent at low input energies (linear regime), whereas the transmittance must drop with increasing input energy (nonlinear regime). There are several physical processes to be exploited for this purpose. For example, optical limiting that is due to two-photon absorption, photorefractive light scattering, light-induced domain reorientation in liquid crystals, and thermal effects in carbon-black suspensions and carbon nanotubes has been reported. For an overview of various physical processes used for optical limiting see, e.g., the review papers Refs. 1 and 2 and references therein.

Excited-state absorption (ESA) evoked by transitions from one excited state to a higher one represents another well-studied mechanism for nonlinear absorption.[3–20] For passive optical limiting applications, the situation that we are primarily concerned with occurs when the ESA cross section is higher than that of the ground state. Then the transmittance of the material will decrease with increasing input. Such materials are called *reverse* saturable absorbers (RSA's). An important feature of RSA's is that the ESA cross section can be much larger [$\sigma_{ex}/\sigma_g \sim 10-30$ (Ref. 10)] than the ground-state absorption cross section. Because the lifetimes of the excited states can be fairly long, the material can exhibit nonlinear absorption over a wide range of input pulse lengths. Some RSA materials exhibit optical limiting properties over a broad spectral range extending into the near infrared.[20] All these features make RSA's remarkable candidates for passive optical limiting. RSA has been observed in several materials, including porphyrins, cyanines, phthalocyanines, naphthalocyanines, fullerenes, metal cluster compounds, doped polymers, and solgel materials (for an overview, see Ref. 10 and references therein).

As follows from the very nature of ESA, the absorptive properties of the material are determined by the population densities of the ground and excited states. The population densities, in turn, depend on the parameters of the nonlinear medium as well as on the laser pulse characteristics. All these parameters influence multilevel rate equations.[3–19] For most cases, a five-level model[4–7,10,12,13,15–19] describes population dynamics with reasonable accuracy, except for extremely high fluence inputs. However, these rather complicated dependencies make it difficult to determine optimum conditions for efficient nonlinear absorption.

Although extensive numerical calculations[13–15] provide useful insight into the population dynamics, a complete scan of all the parameter space by means of a direct numerical integration of the governing equations is difficult to implement and to analyze. However, analytical results would allow us to understand the effect of each parameter and would therefore considerably simplify the optimization problem. The dynamical equations for RSA's, however, do not permit a straightforward analytical treatment. Until now most cases of interest have been treated numerically,[7–9,12–16] whereas an analytical description could be extended only to several cases. Apart from a simplified model (two-level rate equations),[3,4] analytical description was done only either for the stationary regime (pulse lengths are much longer than the excited-state lifetimes)[12,14,19] or for a constant excitation (rectan-

gular input pulses)[10,11,18,19] that only approximately models realistic laser outputs. As was emphasized in Ref. 17, accounting for the shape of the leading edge of the laser pulse is essential for practical applications. In addition, understanding the population dynamics for realistic input pulses is key in estimating the effects of other absorbing mechanisms such as saturable absorption and two- and three-photon absorption.[21]

In this paper we present an approach to accurately describing the population dynamics and therefore the nonlinear absorption of optically thin RSA materials, taking into account the temporal shape of the incident laser pulse. The paper is organized as follows: In Section 2 we introduce rate equations and discuss important parameters and normalizations. In Section 3 we outline the method of performing a dynamical analysis for various regimes of excitation. The general solution is then analyzed for the case of incident pulses of various temporal lengths, and the results are compared with numerical data. The consequences for efficient nonlinear absorption and validity ranges of the approximations are discussed in Section 4, and Section 5 concludes the paper.

2. RATE EQUATIONS AND NORMALIZATIONS

Our analysis is based on a five-level model for ESA[4–7,10,12,13,15–19] that is schematically shown in Fig. 1. The chromophore molecules in the ground state (0) absorb photons and transit to the first excited (singlet) state (1; for practical estimations one can neglect ultrafast relaxation of vibronic sublevels). Molecules from the first excited state can transit to the triplet state (3) within the intersystem crossing lifetime τ_{13} or relax back to the ground state within the time τ_{10}. Additionally, RSA molecules in the singlet and triplet excited states can further absorb photons and be promoted to the upper excited-state levels (2, 4). The transmittance of an optically thin material is calculated from the propagation equation[3,4,7–19]

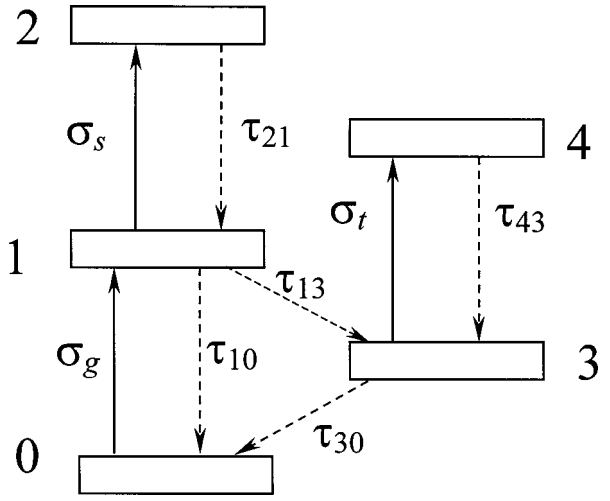

Fig. 1. Schematic diagram of the five-level model of ESA: 0, ground state; 1, 2, excited singlet states; 3, 4, triplet states.

$$\frac{dI(z,t)}{dz} = -I(z,t)[\sigma_g N_0(I,t) + \sigma_s N_1(I,t) + \sigma_t N_3(I,t)], \quad (1)$$

where z denotes the propagation length, $I(z,t)$ is the irradiance of the incident pulse, σ_g is the ground-state absorption cross section, σ_s and σ_t are the singlet and the triplet excited-state cross sections, respectively, and $N_{0,1,3}$ are the respective level population densities (Fig. 1).

Generally, one has to take into account an interplay of populations of all five levels to describe absorption of the RSA material. However, in most cases the lifetimes of upper excited-state levels 2 and 4 are short (<10 ps) compared with the pulse length.[3,4,7,10,12–19] Thus for moderate input irradiance levels the upper singlet- (triplet-) state decay rate $1/\tau_{21}$ ($1/\tau_{43}$) is much larger than the optical pumping rate $\sigma_s I/\hbar\omega$ ($\sigma_t I/\hbar\omega$), so we may neglect the effect of the upper-state populations N_2 and N_4. Under these assumptions we can restrict ourselves to the consideration of a three-level approximation.[7,10–19] Furthermore, because the typical lifetime of the lowest triplet state is of the order of microseconds, whereas we are concerned primarily with nanosecond or shorter input pulses, the triplet-state decay to the ground state may also be ignored. As a result, we arrive at a simplified set of three-level rate equations for the ground-state (N_0), excited-singlet (N_1), and triplet-state (N_3) populations in the form[10,13,15,18]

$$\frac{dN_0}{dt} = -\frac{\sigma_g I(t)}{\hbar\omega} N_0 + \frac{N_1}{\tau_{10}},$$
$$\frac{dN_1}{dt} = \frac{\sigma_g I(t)}{\hbar\omega} N_0 - \frac{N_1}{\tau_1},$$
$$\frac{dN_3}{dt} = \frac{N_1}{\tau_{13}}. \quad (2)$$

Here τ_{10} and τ_{13} are the respective band lifetimes (Fig. 1), $\tau_1^{-1} = \tau_{10}^{-1} + \tau_{13}^{-1}$, and $I(t) = I_0 \hat{f}(t)$ represents the time-dependent input pulse irradiance; $\hat{f}(t)$ is dimensionless.

Equations (2) can be recast into a form convenient for further analysis. To do this we introduce the time $T = t/t_p$ measured in units of input pulse lengths t_p and two key parameters, $A = \sigma_g I_0 t_p/(\hbar\omega)$ and $w = t_p/\tau_1$, that characterize the pulse fluence and temporal pulse length. Then Eqs. (2) take the form

$$\frac{dn_0}{dT} = -f(T)n_0 + w(1-\phi)n_1, \quad (3a)$$

$$\frac{dn_1}{dT} = f(T)n_0 - wn_1, \quad (3b)$$

$$\frac{dn_3}{dT} = w\phi n_1, \quad (3c)$$

where $n_j(T) = N_j(T)/N_0(T_0)$, $j = 0, 1, 3$, are the fractional population densities and T_0 is the time at which the light enters the medium, $f(T) = A\hat{f}(T)$, and $\hat{f}(T)$ is an arbitrary input pulse shape with a unit ampli-

tude. The total population density is conserved: $N_0(T) + N_1(T) + N_3(T) = N_0(T_0)$. Hence, for the fractional population densities, we have

$$n_0(T) + n_1(T) + n_3(T) = 1. \tag{4}$$

The intersystem crossing rate $\phi = \tau_1/\tau_{13}$ $(0 < \phi < 1)$ characterizes a relative transition probability from the first singlet excited state (1) to the ground state (0) and to the lowest triplet state (3); Fig. 1. Below we discuss how Eqs. (3) with $f(T) \neq$ constant can be analyzed.

3. SOLUTION OF TIME–DEPENDENT RATE EQUATIONS

A. General Solution

First we notice that triplet band population n_3 does not enter into Eqs. (3a) and (3b) explicitly, which means that Eq. (3c) is decoupled from the system. Then, introducing an auxiliary function

$$u(T) = n_0(T)\exp\left\{{}^1\!/_2 \int [f(T) + w]\mathrm{d}T\right\}, \tag{5}$$

we can reduce Eqs. (3a) and (3b) to an equivalent linear second-order equation:

$$u'' + P(T)u = 0. \tag{6}$$

Here the double prime denotes a second derivative with respect to T and

$$P(T) = \frac{f'(T)}{2} - \frac{f^2(T)}{4} + w\left(\phi - \frac{1}{2}\right)f(T) - \frac{w^2}{4}. \tag{7}$$

With different forms of $P(T)$, Eq. (6) models various fundamental physical problems such as a parametrically driven oscillator or scattering problem in quantum mechanics. In the stationary Schrödinger equation $P(T)$ relates to the potential function. In our case, this very function $P(T)$, which for brevity we refer to as potential, also determines the whole dynamics of the band populations. It has a complex form that does not allow us to find an exact solution for an arbitrary set of parameters. Thus the main idea of our approach consists in replacing $P(T)$ with a function that closely matches the potential; on the one hand this function allows us to solve Eq. (6) explicitly and on the other hand the deviation of the found solution from the original solution is minimal.

First we briefly outline the steps that one follows to find the general solution to Eq. (6). One of the standard schemes consists in solving a corresponding first-order nonlinear ordinary differential equation that can be obtained from Eq. (6) by the ansatz $v = u'/u$. Then Eq. (6) is transformed into a Riccati equation:

$$v' + v^2 + P(T) = 0. \tag{8}$$

Equation (8) is not integrable in general, but, if any specific solution of this equation $v_0(T)$ is known, the substitution $v = y + v_0(T)$ transforms Eq. (8) into an integrable Bernoulli equation $y' + 2v_0(T)y + y^2 = 0$, which can be further simplified by the substitution $y = 1/\rho$. As a result we get a linear equation $\rho' - 2v_0(T)\rho = 1$ whose solution is $\rho(T) = \{C_0 + \int \exp[-2V_0(T)]\mathrm{d}T\}\exp[2V_0(T)]$, where we have introduced an integral quantity $V_0(T) = \int v_0(T)\mathrm{d}T$. With $\rho(T)$ known we can obtain the dynamics of the ground-state population density by transforming back the variables $\rho \to y \to v \to u$. Ultimately we obtain from Eq. (5)

$$n_0(T) = \left\{C_0 + C_1\int \exp[-2V_0(T)]\mathrm{d}T\right\} \times \exp\left[V_0(T) - \frac{F(T) + wT}{2}\right], \tag{9}$$

where $F(T) = \int f(T)\mathrm{d}T$ and constants $C_{0,1}$ are determined by initial conditions. The population density of the excited singlet state n_1 can be found from either Eq. (9) and (3a) as

$$n_1(T) = \frac{\exp\left[V_0(T) - \dfrac{F(T) + wT}{2}\right]}{w(1 - \phi)} \times \left(C_1\exp[-2V_0(T)] + \left\{C_0 + C_1\int \exp[-2V_0(T)]\mathrm{d}T\right\} \times \left[v_0(T) + \frac{f(T) - w}{2}\right]\right), \tag{10a}$$

or from Eqs. (9) and (3b) as

$$n_1(T) = \left[C_2 + \int f(T)n_0(T)\exp(wT)\mathrm{d}T\right]\exp(-wT), \tag{10b}$$

where C_2 is determined from the initial condition $n_1(T_0) = 0$. If $n_0(T)$ is found approximately, the two expressions for $n_1(T)$ provide different degrees of accuracy; we shall return to this issue below. Ultimately, the triplet band population n_3 is straightforwardly calculated from the conservation law [Eq. (4)].

The solution given by Eqs. (9), (10), and (4) to time-dependent rate equations (3) is general. Each temporal evolution of band populations depends on the shape of the input pulse. To obtain the solution in explicit form, one has to specify the pulse form $\hat{f}(T)$ and find $v_0(T)$. This calculation represents the most difficult task.

As mentioned above, many practically relevant regimes of excitation and pulse shapes permit an approximation of the potential by such a function $\tilde{P}(T)$ that $v_0(T)$ can be found. The form of the approximate potential $\tilde{P}(T)$ depends on the excitation conditions, i.e., on the amplitude and the length of the input laser pulse. Here we analyze different excitation regimes separately.

B. Long Pulses

We start with long input pulses that correspond to the case $w \gg 1$. Then function $P(T)$ acquires a large constant background because of the last term, $-w^2/4$, in Eq. (7). For many practically relevant situations when $\phi \approx 0.5$,[10,15,18] that term makes the only principal contribution to the potential. If such is not the case, the third term in Eq. (7), $w(\phi - 1/2)f(T)$, has also to be taken into account. The first two terms in Eq. (7) scale with A and

A^2, respectively, and, provided that the irradiance is not too high (see Subsection 4.B), do not contribute significantly to $P(T)$. In other words, for long input pulses we can take the approximate potential in the form

$$P(T) \approx \tilde{P}(T) = \left(\phi - \frac{1}{2}\right) f'(T) - \left[\left(\frac{1}{2} - \phi\right) f(T) + \frac{w}{2}\right]^2. \quad (11)$$

The relative error $\Delta P(T)$ occurs then because of the uncompensated first two terms in Eq. (7) and amounts to

$$\Delta P(T) = P(T) - \tilde{P}(T) = (1 - \phi) f'(T) + \phi(\phi - 1) f^2(T). \quad (12)$$

With approximate potential (11), Eq. (8) has a specific solution, $v_0(T) = [(1/2) - \phi] f(T) + w/2$. Then Eq. (6) is solvable, and, together with Eq. (5) and initial conditions $n_0(T_0) = 1$ and $n_1(T_0) = n_3(T_0) = 0$, gives us the formula for the depletion of the ground state:

$$n_0(T) \approx \exp[-\phi \Delta F(T)], \quad (13)$$

where $\Delta F(T) = F(T) - F(T_0) = \int_{T_0}^{T} f(T')\mathrm{d}T'$ is the normalized pulse fluence and we have neglected terms proportional to a small parameter $f(T_0)/w$ and assumed that $\int \exp[-2V_0(T)]\mathrm{d}T \approx \int \exp(-wT)\mathrm{d}T$ in Eq. (9). The evolution of the first excited singlet-state population can be found from formula (13) and Eq. (10a) as

$$n_1(T) \approx \frac{f(T)}{w} n_0(T), \quad (14)$$

and the triplet-state population density is calculated from Eq. (4).

It is important to note that depletion of the ground state under action of long realistic pulses has the same functional dependence on the fluence as in the case of long rectangular pulses studied in Refs. 10, 18, and 19. However, in a quantitative comparison of these two cases one has to be careful with the definition of the pulse length. A rectangular pulse [$I(t) = I_0$ for $-\tau_p \leqslant t \leqslant \tau_p$; $I(t) = 0$ otherwise] and, e.g., a hyperbolic secant pulse $I(t) = I_0 \operatorname{sech}^2 t/t_p$ of the same peak irradiance I_0 have the same total fluence if $\tau_p = 2t_p$. As follows from formula (14), the population dynamics of excited states explicitly depend on the pulse shape.

Taking hyperbolic secant pulses $f(T) = A \operatorname{sech}^2 T$ as an example, we get from formula (13) the evolution of the ground-state population density as

$$n_0(T) \approx \exp[-\phi A(\tanh T + 1)], \quad (15)$$

and for the singlet excited state we obtain from formula (14)

$$n_1(T) \approx \frac{A}{w} \operatorname{sech}^2 T \exp[-\phi A(\tanh T + 1)]. \quad (16)$$

The analytical results given by formulas (15), (16), and (4) are plotted at the left in Fig. 2 together with those obtained by numerical integration of Eqs. (3) for various pulse lengths, peak irradiances, and intersystem crossing rates; the exact and approximate potentials are shown at the right. An appreciable coincidence with the numerics is observed for a wide range of parameters. Evidently, the more exact is the approximation of the potential, the less is the discrepancy between analytical and numerical results. Thus, decreasing pulse length w entails an increase in the relative error $\Delta P/P$, which decreases the accuracy of analytical formulas [cf. Figs. 2(a) and 2(b), where the maximum values of $\Delta P/P$ approximately equal 0.025 and 0.4, respectively]. We have found that for $w > w_{\mathrm{long}} \approx 3$ the discrepancy between the analytical and the numerical results is marginal. To be more specific, the maximum deviation between numerically and analytically calculated fractional populations $\delta n_{\max} = \max_{j,T} |n_j^{\mathrm{an}}(T) - n_j^{\mathrm{num}}(T)|$ is always less than 0.2.

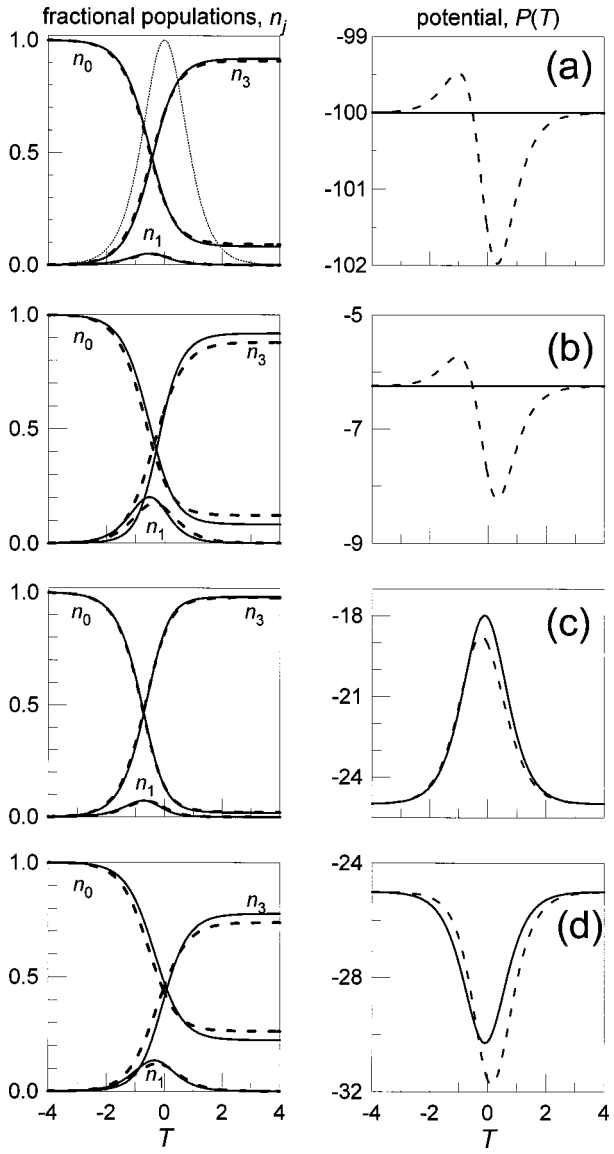

Fig. 2. Dynamics of fractional populations excited by long hyperbolic secant $f(T) = A \operatorname{sech}^2 T$ pulses. The results are obtained by use of analytical formulas (15), (16), and (4) (solid curves) and by numerical integration of the three-level model of Eqs. (3) (dashed curves). The exact potential $P(T)$ given by Eq. (7) (dashed curves) and approximate potential $\tilde{P}(T)$ given by formula (11) (solid curves) are shown at the right. Parameters: (a) $w = 20$, $A = 2.5$, $\phi = 0.5$; (b) $w = 5$, $A = 2.5$, $\phi = 0.5$; (c) $w = 10$, $A = 2.5$, $\phi = 0.8$; (d) $w = 10$, $A = 2.5$, $\phi = 0.3$. The input pulse shape is shown for reference by a dotted line in (a).

Therefore there is a deviation of the fluence effective cross section[10,15,18] calculated with $\sigma_s/\sigma_g = 10$ and $\sigma_t/\sigma_g = 30$ of $\delta\sigma_{ex} = |\sigma_{ex}^{an} - \sigma_{ex}^{num}| < 6\%$. For a nonsymmetric intersystem crossing ($\phi \neq 0.5$), expressions (13) and (14) are more accurate for larger ϕ [cf. Figs. 2(c) and 2(d)], where the error from the term $(1-\phi)f'(T)$ in Eq. (12) is smaller [cf. the respective potentials in Figs. 2(c) and 2(d)]. A tolerable accuracy (e.g., $\delta n_{max} < 0.1$) of analytical formulas with $w \approx 10$ is achieved for $\phi > 0.2$.

C. Short Pulses

For relatively short pulses when $t_p \ll \tau_1$ and consequently $w \ll 1$, the potential is localized; i.e., $P(T)$ has a very small constant background, $-w^2/4$. In this case the less significant contribution is made by the last two terms in Eq. (7). Thus we may take the approximation

$$P(T) \approx \tilde{P}(T) = \frac{f'(T)}{2} - \frac{f^2(T)}{4}. \quad (17)$$

One can prove by a direct substitution that for this case $v_0 = -f(T)/2$ is a solution of Eq. (8). Hence we get from the general solution [Eq. (9)]

$$n_0(T) = \{1 + \epsilon_0[F(T)]\}\exp[-\Delta F(T) - w\Delta T/2], \quad (18)$$

where $\epsilon_0[F(T)] = (w/2)\exp[-F(T_0)]\int_{T_0}^{T}\exp[F(T')]dT'$, $\Delta T = T - T_0$. For example, for hyperbolic secant input pulses $f(T) = A\,\mathrm{sech}^2 T$ Eq. (18) takes the form

$$n_0(T) \approx \left[1 + \frac{w}{4}\Delta S(T)\right] \times \exp[-A(\tanh T + 1) - w(T - T_0)/2], \quad (19)$$

where $\Delta S(T) = S(T) - S(T_0)$ and $S(T) = Ei[A(\tanh T + 1)] - e^{2A}Ei[A(\tanh T - 1)]$, and $Ei(x) = -\int_{-x}^{\infty}[(e^{-q}/q)dq]$ is the exponential integral function.[22] A reasonable approximation of this function for our applications is provided by $Ei(x) \approx \gamma + \ln|x|$ if x is close to zero ($\gamma = 0.577$ is Euler's constant) and $Ei(x) \approx \exp(x)(1 + 1/x)/x$ for large x. It is worth noting that with decreasing pulse length $w \to 0$ we get from Eq. (18) the limit of the slow absorbers defined in Ref. 10.

Unlike in the previous case the use of Eq. (10a) to calculate the singlet-state population density $n_1(T)$ is less appropriate because an additional error is induced by the denominator in Eq. (10a) that is proportional to the small parameter w. Although it is less straightforward, the calculation of $n_1(T)$ with Eq. (10b) is preferable for short input pulses. Thus we substitute $n_0(T)$ given by Eq. (18) into Eq. (10b) and perform the integration, taking a series expansion with respect to w and keeping only linear terms. In fact, we made the same assumption in neglecting the higher-order terms with respect to w in approximate potential (17). The result of integration can be written as

$$n_1(T) = 1 - n_0(T) - n_3(T),$$

$$n_3(T) \approx \frac{w}{2}\{\Delta T - \epsilon_1[F(T)]\}, \quad (20)$$

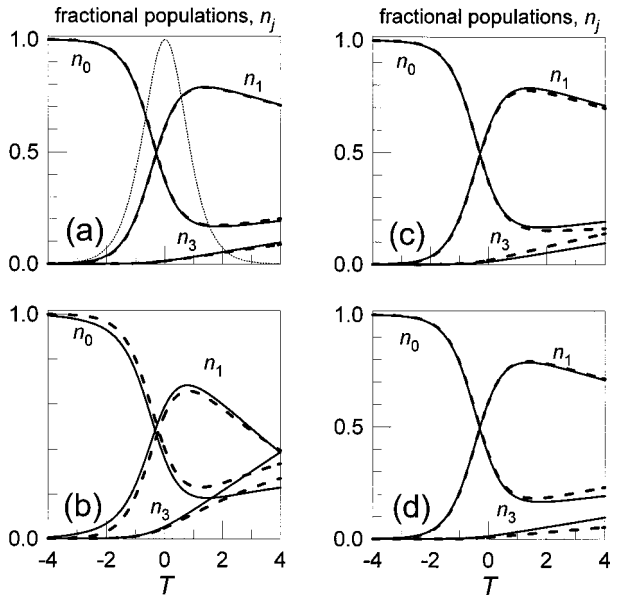

Fig. 3. Dynamics of fractional populations excited by short hyperbolic secant $f(T) = A\,\mathrm{sech}^2 T$ pulses. The results are obtained by use of analytical formulas (19), (21), (solid curves) and by numerical integration of the three-level model of Eqs. (3) (dashed curves). Parameters: (a) $w = 0.05$, $A = 1$, $\phi = 0.5$; (b) $w = 0.2$, $A = 1$, $\phi = 0.5$; (c) $w = 0.05$, $A = 1$, $\phi = 0.8$; (d) $w = 0.05$, $A = 1$, $\phi = 0.3$. The input pulse shape is shown for reference by a dotted curve in (a).

where $\epsilon_1[F(T)] = (w/2)\exp[F(T_0)]\int_{T_0}^{T}\exp[-F(T')]dT'$. For hyperbolic secant pulses the population dynamics of the triplet state in formulas (20) reads as

$$n_3(T) = \frac{w}{4}[2\Delta T - \Delta\bar{S}(T)], \quad (21)$$

where $\Delta\bar{S}(T) = \bar{S}(T) - \bar{S}(T_0)$ and $\bar{S}(T) = Ei[-A \times (\tanh T + 1)] - e^{-2A}Ei[-A(\tanh T - 1)]$.

A comparison of numerical integration of the rate equations with those given by formulas (19) and (21) is made in Fig. 3. For short pulses the analytical results are in excellent agreement with the temporal evolution of the ground- and excited-state populations obtained by direct numerical integration of Eq. (3) [Fig. 3(a)]. However, the error of Eq. (18) and formulas (20) increases with increasing pulse length w [Fig. 3(b)] because of the increasing contribution from the term $-w^2/4$ in Eq. (7). Therefore for intermediate pulse lengths the finite background of the potential begins to matter. We estimate that the upper bound for accurate solutions with this approximation is for input pulse lengths $w < w_{short} \approx 0.3$, i.e., for pulses shorter than several nanoseconds in most RSA materials. The maximum deviations δn_{max} and $\delta\sigma_{ex}$ defined above are then less than 15%.

As follows from the shape of the approximate potential, an increase in pulse peak irradiance A does not have an effect on the accuracy of analytical formulas. Thus the upper boundary for the peak irradiance is restricted only by the validity of the three-level model. It is similarly suspected that approximation (17) imposes less stringent requirements on the intersystem crossing rate [Figs. 3(c) and 3(d)]. Indeed, the term in $P(T)$ that depends on ϕ is multiplied by the small parameter w. We have found

that, for $w = 0.05$ and $A = 1$, $\delta n_{\max}$ and $\delta\sigma_{\mathrm{ex}}$ calculated with formulas (19) and (21) do not exceed 10% for any $0 < \phi < 1$.

D. Intermediate Pulse Length

Analytical solution to Eqs. (3) for intermediate input pulses ($w \approx 1$) represents the most challenging task. Once the two limiting cases of short and long pulses are abandoned and every term in Eq. (7) becomes essential, particular criteria for approximating the solution to Eq. (6) have to be determined. Here we mention only one possible way to approximate the potential. A specific solution to Eq. (8) may be taken as a linear combination of the two approximations considered above, i.e., in the form $v_0(T) = \alpha f(T) + \beta$. This combined approximation results in the following potential:

$$\tilde{P}(T) = -\alpha f'(T) - [\alpha f(T) + \beta]^2. \tag{22}$$

One of the approximation strategies that works for some cases could be minimization of the integral quantity $Q = \int_{-\infty}^{+\infty} |P(T) - \tilde{P}(T)| \mathrm{d}T$ by a choice of the coefficients α and β. The forms of the exact and an approximate potential are shown in Fig. 4. The weighting coefficients α and β are chosen to equalize asymptotic values of the potential that determines β and to set at zero the integral Q that gives us α. The result of numerical integration of Eqs. (3) for $A = 3$, $w = 2$, and $\phi = 0.5$ is presented in Fig. 4 together with the estimation from Eq. (22). The accuracy of the calculated ground-state population remains reasonable, but typically the dynamics of the excited states exhibits a larger discrepancy. This constraint is less significant for RSA's with approximately equal excited singlet and triplet cross sections when the contributions from both excited states to the total nonlinear absorption are approximately the same. Then to calculate the nonlinear transmittance one can take $n_1(T) \approx n_3(T) \approx [1 - n_0(T)]/2$.

4. DISCUSSION

First we estimate real pulse length and irradiance levels that are relevant for the solutions of normalized Eqs. (3) that are described above. Assuming that $\tau_{10} \approx \tau_{13} \approx 10$ ns, which is typical of materials commonly studied for optical limiters,[18] we obtain a lower bound of the pulse length imposed by the condition that $w \gg 1$ (Subsection 3.B) as $t_p \geqslant w_{\mathrm{long}}\tau_{10}(1 - \phi) \approx 15$ ns. For short pulses as described in Subsection 3.C we similarly estimate an upper bound for the pulse length in the framework of the approximation given by formulas (18) and (20) as $t_p \leqslant w_{\mathrm{short}}\tau_{10}(1 - \phi) \approx 1.5$ ns. The lower bound in the case of short pulses is imposed by the validity of the three-level approximation and depends critically on the lifetime of excited singlet states and the input pulse fluence. The results derived in Section 3 allow one to determine basic absorption mechanisms for various regimes of excitation and to calculate the fluence effective cross section that governs nonlinear transmittance of RSA material.

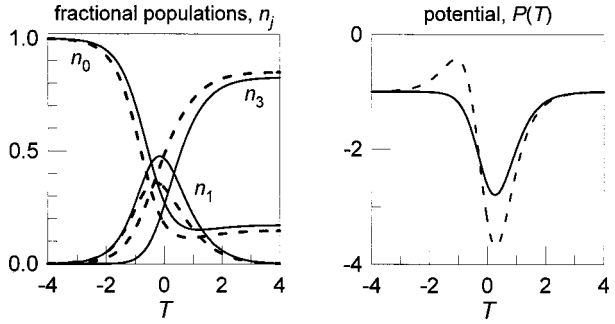

Fig. 4. Population dynamics for a hyperbolic secant pulse $f(T) = A\ \mathrm{sech}^2 T$ of intermediate length. Results obtained with exact [Eq. (7)] and approximate [Eq. (22)] potential are compared. Parameters: $w = 2, A = 3, \phi = 0.5 \rightarrow \alpha = -0.207, \beta = -1$.

A. Effective Excited-State Absorption Cross Sections

There are several quantities that can be considered the effective excited-state absorption cross section.[10,13,15,17,18] The irradiance cross section σ^I_{eff} (Ref. 15) is given by terms in brackets in the propagation equation [Eq. (1)]. The irradiance cross section determines an instantaneous absorption of each portion of the pulse's irradiance and therefore is a function of time. With the normalized quantities introduced, we obtain for the dimensionless (i.e., scaled with the ground-state absorption cross section) irradiance cross section

$$\sigma^I_{\mathrm{eff}}(T) = n_0(T) + \bar{\sigma}_s n_1(T) + \bar{\sigma}_t n_3(T), \tag{23}$$

where we have denoted $\bar{\sigma}_s = \sigma_s/\sigma_g$ and $\bar{\sigma}_t = \sigma_t/\sigma_g$.

Alternatively, propagation equation (1) can be integrated over the whole time span to yield the spatial evolution of the pulse fluence, $\mathcal{F}(t) = \int_{-\infty}^{t} I(z, t')\mathrm{d}t'$ or $\mathcal{F}(T) = \mathcal{F}_s \int_{T_0}^{T} f(T')\mathrm{d}T' = \mathcal{F}_s \Delta F(T)$, where $\mathcal{F}_s = \hbar\omega/\sigma_g = I_0 t_p/A$ is the saturation fluence.[15] Then Eq. (1) is transformed to

$$\frac{\mathrm{d}\mathcal{F}}{\mathrm{d}Z} = -\int_{-\infty}^{t} \sigma^I_{\mathrm{eff}}(t) I(t)\mathrm{d}t = -\int_0^{\mathcal{F}} \sigma^I_{\mathrm{eff}}(\mathcal{F}')\mathrm{d}\mathcal{F}' = -\sigma^{\mathcal{F}}_{\mathrm{eff}}(\mathcal{F})\mathcal{F}. \tag{24}$$

The dimensionless propagation length in Eq. (24), $Z = z\sigma_g N(T_0)$, is a measure of the linear absorption. Indeed, for the linear case we have $n_0(T) \rightarrow 1$ and $n_{1,3}(T) \rightarrow 0$; that is, from Eq. (23) we have $\sigma^I_{\mathrm{eff}}(T) \rightarrow 1$, and Eq. (24) gives $\mathrm{d}\mathcal{F}/\mathrm{d}Z = -\mathcal{F}$. Therefore in the linear regime the fluence absorption is described by $\mathcal{F}(Z) = \mathcal{F}_0 \exp(-Z)$; i.e., the linear transmittance is $T_L = \exp(-Z)$. This means that the value of Z should be small to ensure small linear losses. For instance, $Z = 0.1$ corresponds to approximately 90% linear transmittance. The fluence effective cross section[15] as given by Eq. (24),

$$\sigma^{\mathcal{F}}_{\mathrm{eff}}(F) = \frac{1}{\mathcal{F}} \int_0^{\mathcal{F}} \sigma^I_{\mathrm{eff}}(\mathcal{F}')\mathrm{d}\mathcal{F}', \tag{25}$$

characterizes the nonlinear attenuation of the fluence.

B. Nonlinear Absorption of Long Pulses

As can be inferred from formula (14) for sufficiently long pulses, the population of the first excited singlet state fol-

lows the pulse shape [$n_1(T) \sim f(T)$] and does not grow significantly because of the large denominator w in that formula. Thus for long pulses the main excited state is the triplet state. The excited singlet state acts simply as an intermediate state to promote the excited molecules to the triplet state. Therefore, efficient nonlinear absorption from the triplet state is a dominant mechanism of the RSA and thus requires a large triplet-state cross section σ_t, which is consistent with results of previous studies. Nevertheless, for some cases of interest discussed below, the population of the singlet state and the singlet excited-state cross-section may have important consequences for nonlinear absorption of RSA's and thus for their limiting properties.

From expressions (23), (13), (14), and (4) we obtain the normalized irradiance cross section for the long-pulse approximation as

$$\sigma_{\text{eff}}^{I,\text{long}}(T) = \bar{\sigma}_t + n_0(T)\left[1 - \bar{\sigma}_t + (\bar{\sigma}_s - \bar{\sigma}_t)\frac{f(T)}{w}\right]. \quad (26)$$

This quantity is plotted in Fig. 5(a) as a function of time and peak irradiance A for a fixed pulse length w. As expected, the maximum of the irradiance cross section grows with A and is achieved for later times as the triplet state gets populated. As a limit we have $\sigma_{\text{eff}}^{I,\text{long}} \to \bar{\sigma}_t$. The right-hand side of Eq. (26) can be expressed in terms of the total input fluence $\mathcal{F}$ as

$$\sigma_{\text{eff}}^{I,\text{long}}(\mathcal{F}) = \bar{\sigma}_t + \left[1 - \bar{\sigma}_t + \frac{\bar{\sigma}_s - \bar{\sigma}_t}{w\mathcal{F}_s}\frac{d\mathcal{F}}{dT}\right]\exp\left(-\phi\frac{\mathcal{F}}{\mathcal{F}_s}\right). \quad (27)$$

Assuming as before that the pulse shape is $f(T) = A\,\text{sech}^2 T$ and performing the integration in Eq. (25) with Eq. (27), we end up with the expression for the fluence cross section:

$$\sigma_{\text{eff}}^{F,\text{long}}(\mathcal{F}) = \bar{\sigma}_t + (1 - \bar{\sigma}_t)\frac{\mathcal{F}_s}{\phi\mathcal{F}} \times [1 - \exp(-\phi\,\mathcal{F}/\mathcal{F}_s)] + \frac{2(\bar{\sigma}_s - \bar{\sigma}_t)}{w\phi}\frac{\mathcal{F}_s}{\phi\mathcal{F}} \times \left[2\frac{\exp(-\phi\mathcal{F}/\mathcal{F}_s) - 1}{\phi\mathcal{F}/\mathcal{F}_s} + \exp(-\phi\mathcal{F}/\mathcal{F}_s) + 1\right]. \quad (28)$$

It is convenient to introduce a dimensionless ratio $Y = \phi\mathcal{F}/\mathcal{F}_s$ to write the differential equation for the fluence transmittance [Eq. (24)] in a more compact form:

$$\frac{dY}{dZ} = (\bar{\sigma}_t - 1)[1 - \exp(-Y)] - \bar{\sigma}_t Y - \mu\left[2\frac{\exp(-Y) - 1}{Y} + \exp(-Y) + 1\right], \quad (29)$$

where $\mu = 2(\bar{\sigma}_s - \bar{\sigma}_t)/w\phi$. It is worth noting that Eq. (29) without the third term on the right-hand side,

$$\frac{dY}{dZ} = (\bar{\sigma}_t - 1)[1 - \exp(-Y)] - \bar{\sigma}_t Y, \quad (30)$$

appears in the rectangular pulse approximation where the singlet-state population has been neglected[18] as well as in the fast absorber approximation for very short pulses[10] with $Y = \mathcal{F}/\mathcal{F}_s$ and $\bar{\sigma}_t$ replaced with $\bar{\sigma}_s$. Hence the last term in Eq. (29) is responsible for the effects of the pulse shape and the population of the singlet state. It is clear that for either very long pulses, $w \gg 1$, or approximately equal excited-state cross sections $\sigma_s \approx \sigma_t$, this term can be neglected. However its effect becomes substantial as the pulse length gets shorter, for small intersystem crossing rates ($\phi < 0.5$) or large σ_s compared to σ_t. To illustrate this behavior we compare the numerical solutions to Eqs. (29) and (30) for two sets of parameters. The transmitted fluence $\mathcal{F}(Z)/\mathcal{F}(0)$ is shown in Fig. 6 as a function of normalized propagation length Z with a fixed input fluence $\mathcal{F}(0)/\mathcal{F}_s = 5$. This comparison provides useful insight into the limiting properties of RSA materials and shows that, for some cases [e.g., Fig. 6(b)], accounting for the pulse shape becomes essential. In fact, the smallness of the factor μ in Eq. (29) determines the applicability boundaries of the approximation [Eq. (30)] discussed in Refs. 10 and 18. Hence analytical expressions (24)–(29) provide quantitative estimations of the nonlinear absorption of long pulses and show when the population of the singlet excited state must be taken into account.

To verify the above results we perform a numerical integration of the full system of partial differential equations, solving the equations for the populations dynamics [Eqs. (3)] and the propagation equation together. For this we rewrite Eq. (1) in the same normalization as is taken for Eqs. (3), namely,

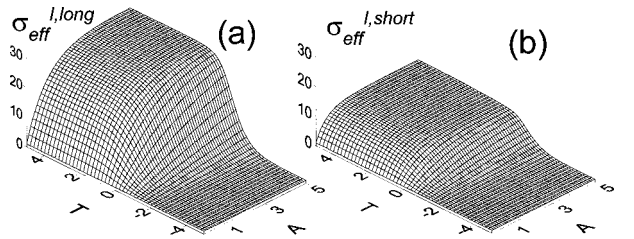

Fig. 5. Irradiance effective cross section σ_{eff}^{I} given by Eq. (23) obtained with analytical formulas for (a) long, $w = 10$, and (b) short, $w = 0.05$, input pulses. Parameters: $\bar{\sigma}_s = 10$, $\bar{\sigma}_t = 30$, $\phi = 0.5$; the pulse shape is a hyperbolic secant.

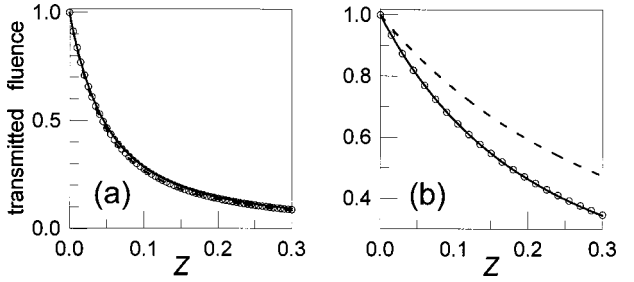

Fig. 6. Transmitted fluence $\mathcal{F}(Z)/\mathcal{F}(0)$ calculated with Eq. (29) (solid curves) and with Eq. (30) (dashed curve), $\mathcal{F}(0)/\mathcal{F}_s = 5$. The results obtained from the numerical integration of the full system of partial differential equations (3) and (31) are shown by circles. Parameters: (a) $\bar{\sigma}_s = 10$, $\bar{\sigma}_t = 30$, $w = 10$, $\phi = 0.5$; (b) $\bar{\sigma}_s = 20$, $\bar{\sigma}_t = 5$, $w = 7.5$, $\phi = 0.3$.

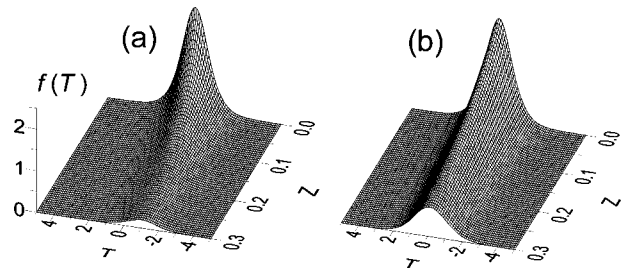

Fig. 7. Numerical integration of the full system of Eqs. (3) and (31). The initial normalized shape of the pulse is $f(T) = A\,\mathrm{sech}^2 T$, $A = 2.5$. Parameters correspond to those of Fig. 6.

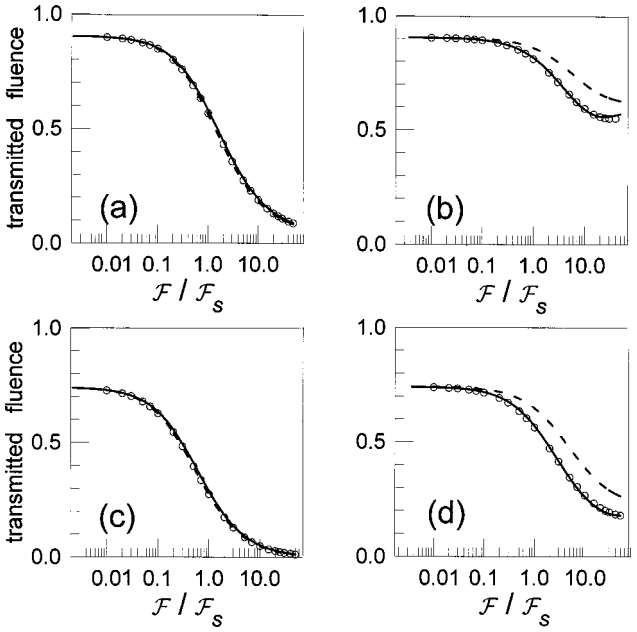

Fig. 8. Transmitted fluence $\mathcal{F}(Z)/\mathcal{F}(0)$ as a function of initial fluence $\mathcal{F}(Z=0)/\mathcal{F}_s$ for a fixed linear transmittance (a), (b) $Z = 0.1 \rightarrow T_L = 0.9$ and (c), (d) $Z = 0.3 \rightarrow T_L = 0.74$. Solid and dashed curves, results of integration of Eqs. (29) and (30), respectively. Circles, numerical solutions of the rate and the propagation equations (3) and (31). Parameters: (a), (c) $\bar{\sigma}_s = 10$, $\bar{\sigma}_t = 30$, $w = 10$, $\phi = 0.5$; (b), (d) $\bar{\sigma}_s = 20$, $\bar{\sigma}_t = 5$, $w = 7.5$, $\phi = 0.3$.

$$\frac{\mathrm{d}f(Z,T)}{\mathrm{d}Z} = -\sigma^I_{\mathrm{eff}}(T) f(Z,T), \tag{31}$$

where normalized propagation length Z was introduced in Eq. (24) and the irradiance cross section $\sigma^I_{\mathrm{eff}}(T)$ is given by Eq. (23). The irradiance profiles obtained from the numerical integration of the system [Eqs. (3) and (31)] are shown in Fig. 7, whereas the corresponding total pulse fluence is depicted in Fig. 6.

To study the dependence of the nonlinear transmittance on the input fluence we plot the transmitted fluence as a function of the initial fluence $\mathcal{F}(Z=0)/\mathcal{F}_s$ for two values of linear transmittance $T_L = 0.9$, i.e., $Z = 0.1$ [Figs. 8(a) and 8(b)] and $T_L = 0.74$, i.e., $Z = 0.3$ [Figs. 8(c) and 8(d)]. Again by comparing Fig. 8(a) with Fig. 8(b) or Fig. 8(c) with Fig. 8(d)]. one can see that taking the pulse shape into account can be important for $\mu \gg 1$. We mention that for high input fluence levels the predictions of Eq. (29) start to deviate from the numerical solution of the full system of Eqs. (3) and (31). This is so because the error of approximation of the potential [Eq. (12)] grows with large irradiances A. Comparing Fig. 8(a) with Fig. 8(c) or Fig. 8(b) with Fig. 8(d), one can conclude that the input fluence level required for strong nonlinear absorption depends on the corresponding linear losses. Thus, e.g., to get $T_{NL} = 0.1$ with the parameters that correspond to those of Figs. 8(a) and 8(c), one needs $\mathcal{F} \approx 33\mathcal{F}_s$ with $T_L = 0.9$ and only $\mathcal{F} \approx 4\mathcal{F}_s$ with $T_L = 0.74$. This gain, however, is taken at the cost of increased linear losses that diminish the figure of merit of the optical limiter. Thus there is a trade-off between allowed linear losses and required input fluence.

C. Nonlinear Absorption of Short Pulses

As can be seen from formulas (18) and (20), absorption of short (less than 1-ns) pulses is a different process. Now the singlet and the triplet states interchange their roles [a rough estimation of formula (20) results in $n_1(T) \approx 1 - n_0(T)$]. Thus the maximum of the irradiance cross section σ^I_{eff} is close to $\bar{\sigma}_s$ [Fig. 5(b)]. The marginal effect of the triplet state on the population dynamics can be anticipated because the intersystem crossing rate ϕ does not enter into the expressions for the population evolution [formulas (18) and (20)]. As in the previous case of long input pulses, the formula for the population dynamics of the ground state (18) predicts the population's exponential depletion. The integral terms $\epsilon_{0,1}[F(T)]$ in formulas (18) and (20) [or alternatively terms proportional to $\Delta S(T)$ and $\Delta\bar{S}(T)$ in Eqs. (19) and (21)] are not essential as far as the initial evolution of the ground- and excited-state populations is concerned. However, they accurately predict the subsequent depletion of the singlet-state population (Fig. 3). This is the crucial difference between the population dynamics of short and long pulses. Under the action of long pulses the excited-state population saturates to the value $n_3^{\mathrm{sat}} \approx 1 - \exp(-2\phi A)$ (Fig. 2). But formulas (18) and (20) do not describe the saturation of the ground-state population at large times because the effect from the neglected nonzero background of the potential $-w^2/4$ accumulates with time.

The error of the analytical formulas manifests itself at large times ($T > 2$ in Fig. 3). However, knowing the value of the error is not critical for calculation of the nonlinear absorption because in the expression for the effective absorption cross section we multiply population densities by the pulse shape, which is essentially zero for large T [Fig. 3(a)]. For this reason the effect of finite pulse length is less important for the short pulses than for the long ones considered above. The onset of the triplet-state buildup does not have a significant effect on the nonlinear absorption because it appears in the differential equation for the fluence transmittance as a small parameter $(\bar{\sigma}_s - \bar{\sigma}_t) w \mathcal{F}/\lambda$; for hyperbolic secant pulses we found that $\lambda > 8$. This means that in the whole validity range of the short-pulse approximation (Subsection 3.C), $w < w_{\mathrm{short}}$, the RSA material may be considered slow (see Ref. 10), and one can use Eq. (30) with $Y = \mathcal{F}/\mathcal{F}_s$ and $\bar{\sigma}_t$ replaced with $\bar{\sigma}_s$ to calculate the fluence transmittance with good accuracy. The results of numerical integration of rate equations (3) and propagation equation (31) are shown in Fig. 9 for two values of the pulse length that cor-

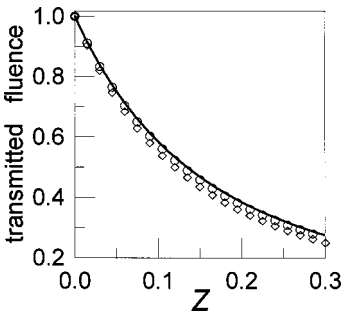

Fig. 9. Transmitted fluence $\mathcal{F}(Z)/\mathcal{F}(0)$ for absorption of short pulses. Solid curve, prediction of the slow- absorber approximation [Eq. (30)]. Numerical integration of Eqs. (3) and (31) is shown by circles for $w = 0.05$ and by diamonds for $w = 0.2$. Parameters: $A = 1 \rightarrow \mathcal{F}/\mathcal{F}_s = 2$, $\phi = 0.5$; initial irradiance profile, $f(T) = A \operatorname{sech}^2 T$.

respond to parameters of Figs. 3(a) and 3(b). In both cases the slow-absorber approximation [Eq. (30)] works fairly well. However, for $w > w_{\text{short}}$ the effect of the triplet-state population may not be negligible.

D. Application for Numerical Algorithms

Another important application of the analytical formulas obtained is their integration into numerical algorithms to model optical beam propagation through a nonlinear medium.[14–16] Usually the whole integration of the system of partial differential equations is split into two steps. At the first step the populations are calculated at all times and all spatial coordinates of the beam. At the second step propagation equation (31) is solved for a thin spatial slice. The spatial distribution of the irradiance computed in this step is then used as a boundary condition for the next spatial slice.[14] The first step represents the most time-consuming operation. This is especially critical if the spatial beam distribution lacks radial symmetry. The numerical integration at the first step can be replaced by the evaluation of analytical expressions (13), (14), and (4) or (18) and (20). The population densities are then calculated for any spatial coordinate for which the irradiance enters the analytic formula merely as a parameter $I = I(x, y)$. Depending on the numerical algorithm implemented, a reduction in computational time by as much as an order of magnitude is expected.

5. CONCLUSIONS

To describe consistently the nonlinear absorption of intense laser pulses, one must take into account the temporal pulse shape to study the dynamics of the ground- and excited-state populations. In the framework of the three-level approximation of the five-level model we have developed an approach that allows one to calculate accurately the temporal evolution of the ground and excited states induced by long ($t_p > 10$-ns) and by short ($t_p < 1$-ns) input pulses. We also discussed a possible strategy for calculating population dynamics for an intermediate case ($1\ \text{ns} < t_p < 10\ \text{ns}$). The analytical predictions agree well with direct numerical integration of both the three-level rate equations and the full system of rate equations and the propagation equation. For realistic input pulses, boundaries when the approximation of slow absorbers may be used are determined. For long pulses we also find criteria for situations in which the population of the singlet excited state may be neglected. With the transmittance calculated as a function of material and pulse parameters one can follow the optimization criteria developed in Refs. 15 and 17 to derive desirable density profiles of graded density limiters or calculate the distance between absorbing elements of tandem limiters that accounts for a particular pulse shape. Additionally, one may use the formulas obtained to fit data from Z-scan[23] or single and double pump–probe measurements[24,25] to determine values of ground- and excited-state cross sections. The analysis demonstrated can also be extended toward absorption of input laser pulses with high repetition rates to explain recently observed effects of the intensity threshold for optical limiting.[26] Finally, the time consumption of numerical beam propagation codes for optically thick materials can be considerably reduced when analytical formulas are used instead of numerical solution of the corresponding system of ordinary differential equations at each spatial propagation step.

ACKNOWLEDGMENTS

The authors gratefully acknowledge the support of the U.S. Office of Naval Research (grant N00014-97-1-0936) and the U.S. Naval Air Warfare Center Joint Service Agile Program (contract N00421-98-C-1327).

A. Kobyakov's e-mail address is andrey @mail.creol.ucf.edu.

REFERENCES

1. L. W. Tutt and T. F. Boggess, "A review of optical limiting mechanisms and devices using organics, fullerenes, semiconductors and other materials," Prog. Quantum Electron. **17**, 299–338 (1993).
2. E. W. Van Stryland, D. J. Hagan, T. Xia, and A. A. Said, "Application of nonlinear optics to passive optical limiting," in *Nonlinear Optics of Organic Molecules and Polymers*, H. S. Nalwa and S. Miyata, eds. (CRC Press, New York, 1997), pp. 840–860.
3. K. R. Welford, S. N. R. Swatton, S. Hughes, S. J. Till, G. Spruce, R. C. Hollins, and B. S. Wherrett, "Nonlinear absorption in organic dyes," Mater. Res. Soc. Symp. Proc. **374**, 239–256 (1995).
4. D. G. Mclean, R. L. Sutherland, M. C. Brant, D. M. Brandelik, P. A. Fleitz, and T. Pottenger, "Nonlinear absorption study of a C_{60}–toluene solution," Opt. Lett. **18**, 858–860 (1993).
5. J. W. Perry, K. Mansour, Y. S. Lee, X. L. Wu, P. V. Bedworth, C. T. Chen, D. Ng, S. R. Marder, P. Miles, T. Wada, M. Tian, and H. Sasabe, "Organic optical limiter with a strong nonlinear response," Science **273**, 1533–1536 (1996).
6. J. S. Shirk, R. G. S. Pong, S. R. Flom, F. J. Bartoli, M. E. Boyle, and A. W. Snow, "Lead phthalocyanine reverse saturable absorption optical limiters," Pure Appl. Opt. **5**, 701–707 (1996).
7. J. Barroso, A. Costela, I. Garcia-Moreno, and R. Sastre, "Wavelength dependence of the nonlinear absorption properties of laser dyes in solid and liquid solutions," Chem. Phys. **238**, 257–272 (1998).
8. H. Stiel, A. Volkmer, I. Rückmann, A. Zeug, B. Ehrenberg, and B. Röder, "Non-linear and transient absorption spectroscopy of magnesium(II)-tetrabenzoporphyrin in solution," Opt. Commun. **155**, 135–143 (1998).

9. J. Oberle, L. Bramerie, G. Jonusauskas, and C. Rulliere, "Optical-limiting properties of a push–pull diphenylbutadiene," Opt. Commun. **169**, 325–332 (1999).
10. J. W. Perry, "Organic and metal-containing reverse saturable absorbers for optical limiters," in *Nonlinear Optics of Organic Molecules and Polymers*, H. S. Nalwa and S. Miyata, eds. (CRC Press, New York, 1997), pp. 813–840.
11. M. Hercher, "An analysis of saturable absorbers," Appl. Opt. **6**, 947–954 (1967).
12. C. Li, L. Zhang, M. Yang, H. Wang, and Y. Wang, "Dynamic and steady-state behaviors of reverse saturable absorption in metallophthalocyanine," Phys. Rev. A **49**, 1149–1157 (1994).
13. X. Shang, Y. Liu, G. Tang, G. Zhang, and W. Chen, "Optical nonlinearities of hypocrellin A with the excitation of nanosecond pulses," J. Opt. Soc. Am. B **15**, 1502–1511 (1998).
14. S. Hughes, J. M. Burzler, and T. Kobayashi, "Modeling of picosecond-pulse propagation for optical limiting applications in the visible spectrum," J. Opt. Soc. Am. B **11**, 2925–2929 (1997).
15. T. Xia, D. J. Hagan, A. Dogariu, A. Said, and E. W. Van Stryland, "Optimization of optical limiting devices based on excited state absorption," Appl. Opt. **36**, 4110–4122 (1997).
16. D. I. Kovsh, S. Yang, D. J. Hagan, and E. W. Van Stryland, "Nonlinear optical beam propagation for optical limiting," Appl. Opt. **38**, 5168–5180 (1999).
17. P. Miles, "Bottleneck optical limiters: the optimal use of excited-state absorbers," Appl. Opt. **33**, 6965–6979 (1994).
18. P. Miles, "Bottleneck optical pulse limiters revisited," Appl. Opt. **38**, 566–570 (1999).
19. K. Dou, X. Sun, X. Wang, R. Parkhill, Y. Guo, and E. T. Knobbe, "Optical limiting and nonlinear absorption of excited states in metalloporphyrin-doped sol gels," IEEE J. Quantum Electron. **35**, 1004–1014 (1999).
20. S. R. Mishra, H. S. Rawat, and S. C. Mehendale, "Reverse saturable absorption and optical limiting in C_{60} solution in the near-infrared," Appl. Phys. Lett. **71**, 46–48 (1997).
21. F. Li, Y. Song, K. Yang, S. Liu, C. Li, Y. Wu, X. Zuo, C. Yu, and P. Zhu, "Determination of nonlinear absorption mechanisms using a single pulse width laser," J. Appl. Phys. **82**, 2004–2006 (1997).
22. M. Abramowitz and I. Stegun, *Handbook of Mathematical Functions* (Dover, New York, 1972).
23. E. W. Van Stryland and M. Sheik-Bahae, "Z-scan," in *Characterization Techniques and Tabulations for Organic Nonlinear Optical Materials*, M. G. Kuzyk and C. W. Dirk, eds. (Marcel Dekker, New York, 1998), pp. 655–692.
24. J. Schell, D. Ohlmann, D. Brinkmann, R. Levy, M. Joucla, J. L. Rehspringer, and B. Honerlage, "Reverse saturable absorption in C_{60}-doped porous glasses studied by single- and double-pulse pump–probe experiments," J. Chem. Phys. **111**, 5929–5937 (1999).
25. S. N. R. Swatton, K. R. Welford, R. C. Hollins, and J. R. Sambles, "A time resolved double pump–probe experimental technique to characterize excited-state parameters of organic dyes," Appl. Phys. Lett. **71**, 10–12 (1997).
26. J. Schell, D. Brinkmann, D. Ohlmann, B. Honerlage, R. Levy, M. Joucla, J. L. Rehspringer, J. Serughetti, and C. Bovier, "Optical limiting properties and dynamics of induced absorption in C_{60}-doped solid xerogel matrices," J. Chem. Phys. **108**, 8599–8604 (1998).